Computers & Fluids 116 (2015) 74–87

Contents lists available at ScienceDirect

Computers & Fluids

journal homepage: www.elsevier.com/locate/compfluid

A scalable coupled surface–subsurface flow model

T. De Maet [a,b,*], F. Cornaton [c], E. Hanert [a,b]

[a] Earth and Life Institute, Environmental Sciences, Université catholique de Louvain, B-1348 Louvain-la-Neuve, Belgium
[b] Georges Lemaître Centre for Earth and Climate Research, Université catholique de Louvain, B-1348 Louvain-la-Neuve, Belgium
[c] Groundwater Modelling Centre DHI-WASY, Berlin, Germany

ARTICLE INFO

Article history:
Received 30 August 2013
Received in revised form 9 February 2015
Accepted 26 March 2015
Available online 16 April 2015

Keywords:
Surface–subsurface coupling
Implicit–explicit time integration
Parallel scaling

ABSTRACT

The coupling of physically-based models for surface and subsurface water flows is a recent concern. The study of their interactions is important both for water resource management and environmental studies. However, despite constant innovation, physically-based simulations of water flows are still time consuming. That is especially problematic for large and/or long-term studies, or to test a large range of parametrizations with an adjoint model. As the current trend in computing sciences is to increase the computational power with additional computational units, new model developments are expected to scale efficiently on parallel infrastructures. This paper describes a coupled surface–subsurface flow model that combines implicit and explicit time discretizations for the surface and subsurface dynamics, respectively. Despite that the surface flow has a faster dynamics than the subsurface flow, we are able to use a unique nearly-optimal time step for each submodel, hence improving the resources use. The surface model is discretized with an implicit control volume finite element method while the subsurface model is solved by means of an explicit discontinuous Galerkin finite element method. The surface and subsurface models are coupled by weakly imposing the continuity of water pressure. By imposing a threshold on the influence coefficients of the control volume finite element method, we can prevent the occurrence of unphysical fluxes in anisotropic elements. The proposed coupling is shown to produce results similar to state-of-the-art models for four different test cases while achieving better strong and weak scalings on up to 192 processors.

1. Introduction

The anthropogenic impact on the environment intensifies continuously with the expansion of the population and the development of its standard of living. To study how human activities influence its surrounding environment, it is important to fully understand the biogeochemical exchanges across the biosphere. Such exchanges are mainly driven by surface and subsurface water flows, which are difficult to predict without appropriate tools. Numerical models are increasingly used for this purpose.

Physically-based models are competing with statistically-based models. The formers are based on complex mathematical equations that can be difficult to parametrize [1] but with the added value of an understanding of the underlying processes. The laters, based on simple generic formulas, can provide an easy and precise fit with observations data but lack of flexibility when a change occurs in the system [2]. It is possible to mix both approaches with an uncertainty analysis to assess the variability of the results [3]. The main sources of uncertainty of physically-based models are the physical model hypotheses, the mathematical approximations, the numerical discretization, the heterogeneity and variability of the parameters, and the calibration of non-linear models with uncertain measures.

In a physically-based model of the terrestrial water cycle, the processes are usually modeled by means of the shallow water equations for the surface flows and the Richards' equation for the subsurface flows. The shallow water equations are a convenient 2D approximation of the full 3D Navier–Stokes equations when the water height is small, which is the case for surface flows. It can be complemented by additional 1D equations for rivers and channels to handle the jump in the physical process scales. The Richards' equation approximates the soil as a porous medium with highly non-linear parameters. It assumes an isothermal and laminar flow with no chemical gradients or inertial forces and water as the unique fluid phase, hence neglecting the air component [1]. It can be complexified by adding hysteresis, fractures, multiple phases or macropores, although those extensions are difficult to

* Corresponding author at: Earth and Life Institute, Environmental Sciences, Université catholique de Louvain, B-1348 Louvain-la-Neuve, Belgium. Tel.: +32 10 47 36 11.
E-mail address: thomas.demaet@uclouvain.be (T. De Maet).

http://dx.doi.org/10.1016/j.compfluid.2015.03.028
0045-7930/

spatialize and parametrize. Since the physical complexity of the shallow water equations goes beyond what is required for surface–subsurface flow interactions, simpler models are generally used. The most popular ones are the non-inertia or diffusive wave model and the kinetic wave model. Some simplified approaches based on the kinetic wave equation are going further in the approximations, simulating the surface water via a tree-structured network of water reservoirs, following the topographical slopes [4]. While being fast, this method is based on strong underlying hypothesis and is hence inappropriate for natural reservoirs. Among the many existing approaches [5–7], a state-of-the art method to discretize the non-inertia equation is the control volume finite element (CVFE) method, also called the influence coefficient method [8–12]. This method applies upwind fluxes between the nodes of a mesh element. Its main advantage over the classical continuous Galerkin formulation is to avoid the issues related to zero or negative water depths. As the non-inertia equation is nearly elliptic when the water height becomes significant, an implicit time integration scheme is recommended.

The numerical discretization of the Richards' equation has been extensively studied, as it presents various numerical difficulties such as unphysical oscillations, mass conservation errors or a lack of robustness. These issues can be partly circumvented by carefully selecting the non-linear solver [13,14] as well as the space discretization [9,15,16]. Most Richards' equation models rely on implicit time integration schemes and hence present convergence issues [17] or sub-optimal scaling on parallel infrastructures [18–23]. The time step of implicit time integration schemes is unrestricted for simple diffusion equations, but the non-linearities of the Richards' equation put an upper limit to it [17]. Recently, De Maet et al. [24] have proposed a model using an explicit time integration scheme and a discontinuous Galerkin (DG) finite element (FE) spatial discretization. Such an approach achieves an optimal strong scaling as it does not require linear or non-linear solvers and hence avoids the associated convergence issues. It relies on the use of slope limiters to increase the scheme robustness and a special DG interface term that allows physical discontinuities in the water content at the elements interface. The interface between two different soils is precisely represented by the DG FE approximation, therefore no mixing between the different properties is necessary as it is the case in continuous Galerkin FE models. A detailed review of Richards' equation models can be found in [16].

In the last decade, the coupling of the shallow water equations and the Richards' equation has been an increasingly active domain of research (see for instance [25] or [26] for an overview). The complexity of studies in this field are mostly due to the fact that surface and subsurface interactions are difficult to measure. Another issue is the difficulty to model water fluxes that often exhibit a large spatial and temporal variability. Indeed, processes occurring at small spatial scales, like river flows, coexist with processes occurring at large spatial scales, like groundwater flows. Similarly, slow processes like the dynamics of the vadose zone coexist with rapid processes like surface runoff.

In a continuous world, when surface water is present, the most physically consistent coupling is to match the hydrostatic pressure of the surface flow with the pressure head of the subsurface flow at the top of the soil layer [18,12]. However, a pressure continuity (PC) coupling strategy would require the soil to be discretized up to the scale of the smallest water fluxes between surface and subsurface, which is rarely feasible in practice because of the associated computational cost. Additionally, the small features of the surface linked to those specific fluxes, such as the microtopography, the surface soil compression and vegetation cover, are often very difficult to estimate. Eventually, such a coupling strategy requires the surface and subsurface models to be connected in one non-linear solver step. The solution is then provided either by iterative coupling methods, which require multiple iterations per time step, or by an implicit time integration scheme, which produces a non-linear system that is often difficult to solve and scales poorly on parallel architectures. Another coupling is the first-order exchange coefficient (FOEC) coupling for which the pressure continuity is weakly imposed [9,10,12]. The FOEC coupling allows the surface and subsurface to be solved separately and it can assume additional sub-scale physics at interfaces. It converges towards the PC coupling when the coefficient tends towards infinity. With an appropriate choice of coefficient it can produce results very close to the PC coupling with enhanced model performances [27,28].

Although the research on coupled surface–subsurface models is well developed, none of the current models achieve an optimal scaling on parallel architectures. For Richards' equation, the parallel efficiency (defined as the fraction of available computational resources fully-used) of a model like PARSWMS is of 75% but it can decrease to 29% in some cases [20]. For the coupled model PARFLOW, the efficiency varies between 40% and 72% [18]. As a general rule of the thumb, performances decrease with the number of computational units and increase with the number of degrees of freedom allocated to each computational unit. This is mainly due to the complexity of the global system solution, which requires many communications to exchange information between subdomains. That amount of communications limits the parallel efficiency, especially when a large number of nodes is involved. Those performances are likely to keep decreasing in the future with the use of newer technologies. Indeed, today new computers increase their power by adding more computational units. That implies a change of paradigm for computational code development as individual computing units are no longer increasing in power. Instead, the number of computing units increases. To use all capabilities of future devices, adapted algorithms have therefore to be developed to achieve efficient parallel codes.

In this paper, we present a coupled surface–subsurface flow model that combines an implicit model for the non-inertia shallow water equation and an explicit model for the Richards' equation [24]. Such an approach allows us to use the same time step for both models, as the slow dynamics of the groundwater requires an explicit time step close to the implicit time step required for convergence of the surface flow non-linear solver. Despite using an implicit scheme for the surface model, the overall scaling is still nearly optimal as the subsurface model generally needs the largest part of the computational resources. The FE method has been selected mostly for its ability to solve the model equations on unstructured meshes, which are well suited to complex geometries such as real catchments. Its CVFE declination for surface flow is close to a finite volume method, increasing first the robustness and then the scheme convergence. Its DG FE declination for subsurface flow allows for physical discontinuities of the water content and for the use of limiters to also increase the scheme robustness. As both the non-inertia and the Richards equations are strongly non-linear, robustness is often favored over precision, which would be achieved for instance by a higher order spatial discretization. The use of similar spatial discretizations for the surface and the subsurface models allows an easier coupling, as each surface element has a unique corresponding subsurface element face. We introduce a flexible coupling approach that lies between an exact surface–subsurface pressure coupling, and the FOEC formulation. This hybrid coupling comes together with the DG FE method when using its Dirichlet boundary condition. It has the advantages to be easier to solve than a direct coupling, as it is less stringent, to converge towards the pressure continuity coupling after a transitory

phase, and to be usable with an explicit time integration scheme. This is not the case of the exact coupling that requires a conjoint implicit solution of both the surface and the subsurface models. A number of numerical examples are provided to highlight the model properties and show how the scaling is affected by the surface and subsurface models.

2. Mathematical formulation

In this section, we give an overview of the subsurface and surface models and describe different approaches to couple these two models.

2.1. Subsurface model

The 3D subsurface model relies on the three-dimensional Richards' equation, which can be expressed as follows:

$$\frac{\partial\theta}{\partial t} = \nabla\cdot(\mathbf{K}\cdot\nabla(\psi - z)) + s, \tag{1}$$

$$\theta = f_\theta(\psi), \tag{2}$$

where θ [L^3L^{-3}] is the volumetric soil water content, ψ [L] is the pressure head, z [L] is the upward positive vertical coordinate, s [T^{-1}] a sink-source term, $\mathbf{K}$[LT^{-1}] the water conductivity tensor and f_θ [–] the retention curve. Eqs. (1) and (2) are complemented with appropriate initial and boundary conditions:

$$\psi = \psi_0, \text{ on } \Omega, \quad t = 0 \tag{3}$$

$$\psi = \psi_D, \text{ on } \Gamma_D, \ t \in [0, t_{end}] \tag{4}$$

$$-(\mathbf{K}\cdot\nabla(\psi - z))\cdot\mathbf{n} = J_N, \text{ on } \Gamma_N, \ t \in [0, t_{end}] \tag{5}$$

with $\mathbf{n}$ [–] the outward normal vector, t_{end} [T] the simulation duration, Ω the computational domain, Γ_D the Dirichlet part of the boundary (where the value ψ_D is imposed) and Γ_N the Neumann part (where the flux J_N is imposed). The constitutive relations defining $\theta = f_\theta(\psi)$ and $\mathbf{K}$ are derived from van Genuchten [29] and Mualem [30]:

$$S_e = \frac{\theta - \theta_r}{\theta_s - \theta_r}, \tag{6}$$

$$S_e = \begin{cases} (1 + |\alpha\psi|^\beta)^{-\nu} & \text{if } \psi \leqslant 0, \\ 1 & \text{if } \psi > 0, \end{cases} \tag{7}$$

$$\mathbf{K} = \mathbf{K}_s S_e^{l_p}\left(1 - (1 - S_e^{1/\nu})^\nu\right)^2, \tag{8}$$

where S_e [–] is the effective saturation, θ_r [L^3L^{-3}] is the residual volumetric water content, θ_s [L^3L^{-3}] is the saturated volumetric water content, $\mathbf{K}_s$ [LT^{-1}] is the anisotropic saturated water conductivity tensor, α [L^{-1}] is a parameter related to the air-entry pressure value, β [–] is a parameter related to the pore-size distribution, and $\nu = 1 - 1/\beta$ [–].

2.2. Surface model

The surface water is modeled with the non-inertia approximation of the shallow water equations. These equations rely on the assumption that the flow aspect ratio is very small. The non-inertia approximation further assumes that inertial terms can be neglected. Gottardi and Venutelli [31] have shown that this approximation is acceptable to simulate runoff flows as it yields results very close to the analytical and numerical solution of the full shallow water equations. The non-inertia approximation reads:

$$\frac{\partial h}{\partial t} - \nabla\cdot\left(h^{3/2}\sqrt{\frac{g}{G}}\frac{\nabla(h+b)}{\sqrt{|\nabla(h+b)|}}\right) = q_s \tag{9}$$

for which the z-axis is defined positive upward, where h [L] is the thickness of the water layer, b [L] is the surface elevation, g [LT^{-2}] is the gravitational acceleration, G [–] a friction coefficient and q_s [LT^{-1}] a source/sink term. G can be expressed as follows:

$$G = \frac{g n_x^2}{h^{1/3}} = \frac{g}{C_x^2} = \frac{f_x}{8} \tag{10}$$

where n_x [$TL^{-1/3}$] is the Manning coefficient, C_x [$L^{1/2}T^{-1}$] is the Chezy coefficient and f_x [–] is the Darcy coefficient.

2.3. Coupling between the surface and subsurface models

The shallow water equations and the Richards' equation are coupled through a boundary condition of the subsurface model, by equating the surface hydrostatic pressure (assumed to be equal to h) and the subsurface pressure head ψ when $h > 0$. To ensure mass-conservation, the interface flux F_{BC} [T^{-1}] is applied to the surface model as a source term through q_s in Eq. (9). The expression of F_{BC} depends on the coupling method. In this study, we will consider two common coupling strategies and then present a new one that combines the two previous ones. Each coupling has its own advantages and drawbacks both in term of numerical discretization and of physical accuracy.

When no ponding occurs, the interface flux is driven by the evapotranspiration. However, over the time scale of a rainfall event the evapotranspiration flux can be neglected as compared to the magnitude of the rain flux. All the test cases presented in this paper are driven by rainfall events and hence neglect evapotranspiration. Of course, evapotranspiration will have to be taken into account to achieve realistic, long-term simulations.

When ponding occurs, two main approaches are commonly used, the PC coupling and the FOEC coupling:

$$F_{BC,PC} = \mathbf{n}\cdot(\mathbf{K}\cdot\nabla(\psi - z)), \tag{11}$$

$$F_{BC,FOEC} = \alpha_{FOEC}(\psi - h), \tag{12}$$

where α_{FOEC} [T^{-1}] is an exchange coefficient. If this coefficient is large, ψ and h quickly converge. If it is small, the two models are almost decoupled. The PC coupling could be viewed as a special case of the FOEC coupling when α_{FOEC} is infinite. This coefficient is able to model surface features different from the bulk of the soil. The flux of Eq. (12) is then viewed as the simplest expression of a Darcy flux. Following the approach of VanderKwaak [9] α_{FOEC} is defined as:

$$\alpha_{FOEC} = K_z\frac{\zeta}{a_s}f^a\chi, \tag{13}$$

where K_z [LT^{-1}] is the soil conductivity in the z direction, ζ [L^{-1}] is the surface exchange interface area to volume ratio, a_s [L] is the surface coupling length scale, f^a [–] is the isotropic porous media area fraction (used only when macropores are considered) and χ [–] is an exchange scaling coefficient. As these parameters are often difficult to estimate and measure in practice, it is usual to use the empirical formula $\alpha_{FOEC_*} = K_z/l_c$ instead of Eq. (13), where l_c [L] is a characteristic length which acts as a fitting parameter [27].

A third approach is to combine the pressure-continuity and FOEC fluxes to obtain a hybrid coupling. The coupling flux is then mathematically expressed as

$$F_{BC,DG} = \sigma_B(\psi - h) + \mathbf{n}\cdot(\mathbf{K}\cdot\nabla(\psi - z)), \tag{14}$$

where σ_B [T^{-1}] is a penalty parameter quite similar to α_{FOEC_*}. On the one hand, the above definition of α_{FOEC_*} involves only parameters that have a physical meaning, although they are often difficult to measure. On the other hand, σ_B is set according to the penalty parameters of the DG space discretization (see Eq. (32)). σ_B is defined by assuming that the soil-surface is like any other inter-element interface within the soil computational domain and is proportional to K_z/l_e, where l_e is a

characteristic length of the two adjacent elements. The difference with the α_{FOEC*} formula is that l_c is generally user-defined while l_e is defined automatically from the model. The interface flux described by Eq. (14) can be viewed as a compromise between the continuous coupling and the FOEC coupling, close to a Robin boundary condition. It is a weak coupling, enhancing the solver convergence, and it converges towards the physical continuity coupling when ψ has reached h. It is consistent with the soil domain discretization described thereafter. Indeed, no specific code was necessary to introduce Eq. (14) as it is already part of the DG FE method when a Dirichet boundary condition is specified.

As a side note we shall point out that the main advantage of the PC coupling is its physical meaning, as water pressure does not exhibit discontinuities. However, as mentioned before, it brings additional numerical issues. Both the FOEC and the hybrid couplings avoid those issues by relaxing the equality constraint with a weak coupling. The coefficient σ_B of the hybrid coupling is coherent with the DG discretization that will be introduced in the next section and is automatically fixed. The constraint at the coupling interface has the same strength that the constraint of the subsurface model at elements interfaces. The result is therefore close to the one obtained with the PC coupling. The FOEC coupling can reach the same goal or can describe near-surface physics, depending on the user-defined parameter l_c. In the present model we do not use the PC coupling. The hybrid coupling is always used, except when additional near-surface physical processes are required (like in Section 4.2). In that case, the FOEC coupling is used and the parameter l_c is calibrated to achieve the best fit with observations.

3. Space and time discretizations

The model equations are now discretized in space and time, before being coupled. We first present the discretization of Richards' equation with a DG FE scheme in space and an explicit scheme in time. We then consider the discretization of the non-inertia approximation of the shallow water equations with a CVFE scheme in space and an implicit scheme in time. Finally, we summarize the entire coupling algorithm.

3.1. Discretization of the subsurface model

Before formally discretizing the subsurface model, the ideas of the resolution procedure are presented for additional clarity. Eq. (1) is usually expressed in two forms, namely the ψ-form and the θ-form:

$$C\frac{\partial\psi}{\partial t} = \nabla\cdot(\mathbf{K}\cdot\nabla(\psi - z)) + s, \tag{15}$$

$$\frac{\partial\theta}{\partial t} = \nabla\cdot\left(\frac{\mathbf{K}}{C}\cdot\nabla\theta - \mathbf{K}\cdot\nabla z\right) + s, \tag{16}$$

where $C(\psi) = df_\theta(\psi)/d\psi$ [L^{-1}]. Eq. (15) is valid everywhere but generally leads to mass conservation issues. Eq. (16) is best suited to dry soils and is not valid in saturated soils. We have adopted the following approach for approximating the subsurface model: (1) solving a modified version of Eq. (15) by initially neglecting the mass-conservation issue, (2) solving Eq. (1) by using the value of ψ from the first step as a predictor, (3) updating the ψ field with $f_\theta^{-1}(\theta)$ [–] in unsaturated areas and (4), if necessary, using a smoother on θ in saturated areas.

The approximation to the step (1) consists in modifying the function C to allow the use of an explicit time integration scheme. Indeed, C (almost) reached 0 in saturated areas and an explicit time integration scheme would require extremely small time steps to remain stable. We therefore make the following approximation:

$$C \simeq \widetilde{C} = \max(C, K/\tau), \tag{17}$$

where K [LT^{-1}] is the largest eigenvalue of conductivity tensor $\mathbf{K}$ and τ [L^2T^{-1}] is a free parameter. In transient situations, we iterate over step (1) to converge towards the exact solution. The iterations on θ in steps (2) and (4) are perfectly mass-conservative. The approximation occurs in the saturated zone but also in a small part of the unsaturated zone where $\widetilde{C} > C$. When an abrupt transition occurs in saturated areas, the algorithm can produce spurious mass fluxes. To correct these in an explicit and mass-conservative way, the following smoother equation is used:

$$\frac{\partial\theta}{\partial t} = \lambda\nabla^2(\theta - f_\theta(\tilde{\psi})), \tag{18}$$

where λ [L^2T^{-1}] is a free parameter and $\tilde{\psi}$ is the value of ψ at the current time step (constant within this equation). The effect of this equation is simply to filter out unwanted variations of θ. Several iterations of this equation can be applied to increase its effect.

Now Eqs. (1), (15) and (18) are discretized in space with the DG FE method. This method is well-suited to represent advection-dominated flows like infiltration fronts. The DG FE method also allows physical discontinuities of θ between soils of different properties, or the use of slope limiters to prevent spurious oscillations. By partitioning the domain Ω into N non-overlapping elements Ω_e with interfaces Γ_e, the spatially and temporally continuous model variables θ and ψ can be approximated by the discrete variables θ^h and ψ^h as

$$\theta(x,y,z,t) \simeq \theta^h(x,y,z,t) = \sum_{j=1}^{N_d}\theta_j(t)\phi_j(x,y,z), \tag{19}$$

$$\psi(x,y,z,t) \simeq \psi^h(x,y,z,t) = \sum_{j=1}^{N_d}\psi_j(t)\phi_j(x,y,z), \tag{20}$$

where N_d [–] is the total number of degrees of freedom (DOF's) and ϕ_j [–] are piecewise first-order Lagrange polynomials defined on each element Ω_e. The jump $[\cdot]$ and averaging $\{\cdot\}$ operators on the interface Γ_e are defined as:

$$[x] \triangleq x^+ - x^-, \qquad \{x\} \triangleq \frac{x^+ + x^-}{2}, \tag{21}$$

where the '+' and '–' superscripts indicate the trace value taken either on one or opposite side of Γ_e. At the boundaries, both operators are defined in terms of an external value derived from the Dirichlet boundary condition. The resulting weak boundary conditions are known to be more stable than strong ones [32,33] and will be used further for the coupling as well. The discrete equations are obtained by deriving the Galerkin formulation of Eqs. (15), (1), and (18) with the basis functions ϕ_i ($1 \leqslant i \leqslant N_d$). The interior penalty DG method is then applied. By using a matrix notation and capitalizing vectors variables, we obtain

$$\widetilde{C}M\frac{d\Psi}{dt} = K\Psi - Z + P, \tag{22}$$

$$M\frac{d\Theta}{dt} = K\Psi - Z + P, \tag{23}$$

$$M\frac{d\Theta}{dt} = \Lambda(\Theta - f_\theta(\tilde{\Psi})) + P_\theta, \tag{24}$$

where the matrices M, K, Λ are obtained by assembling the following element-wise matrices, with n_e the number of nodes per element and $1 \leqslant i, j \leqslant n_e$ over each element e and its neighbors:

$$M_{ij}^e = \langle\phi_i\phi_j\rangle, \tag{25}$$

$$K_{ij}^e = \langle\mathbf{K}\cdot\nabla\phi_i\cdot\nabla\phi_j\rangle - \langle\!\langle\{(\mathbf{K}\cdot\nabla\phi_j)\cdot\mathbf{n}\}[\phi_i]\rangle\!\rangle, \tag{26}$$

$$\Lambda_{ij}^e = \langle\lambda\nabla\phi_i\cdot\nabla\phi_j\rangle - \langle\!\langle\{\lambda\nabla\phi_j\cdot\mathbf{n}\}[\phi_i]\rangle\!\rangle, \tag{27}$$

where $\langle\cdot\rangle$ is defined as $\sum_{e=1}^{N}\int_{\Omega_e}\cdot\,d\Omega$ and $\langle\!\langle\cdot\rangle\!\rangle$ as $\sum_{e=1}^{N}\int_{\partial\Omega_e}\cdot\,d\Gamma$. The vectors Z, P, P_θ are assembled in the same way, with $1 \leqslant i \leqslant n_e$:

$$Z_i^e = \langle \mathbf{K}\cdot\mathbf{z}\cdot\nabla\phi_i + s\phi_i\rangle - \langle\!\langle \{(\mathbf{K}\cdot\mathbf{z})\cdot\mathbf{n}\}[\phi_i]\rangle\!\rangle, \tag{29}$$

$$P_i^e = \sigma\langle\!\langle [\phi_i][\psi^h]\rangle\!\rangle, \tag{30}$$

$$P_{\theta i}^e = \sigma_\theta\langle\!\langle [\phi_i][\theta^h - \theta_{ref}]\rangle\!\rangle, \tag{31}$$

where the penalty parameters σ [T^{-1}] and σ_θ [LT^{-1}] are defined as:

$$\sigma = \frac{4}{l_e}(n_0+1)(n_0+2)K_{sc}, \tag{32}$$

$$K_{sc} = (\mathbf{K}\cdot\mathbf{n})\cdot\mathbf{J}/\|\mathbf{J}\|, \tag{33}$$

$$\mathbf{J} = \mathbf{K}\cdot\nabla(\psi - z), \tag{34}$$

$$\sigma_\theta = \frac{4}{l_e}(n_0+1)(n_0+2)\lambda, \tag{35}$$

with n_0 [–] the order of the FE approximation (in our case $n_0 = 1$), K_{sc} [LT^{-1}] the normal flux-oriented scalar conductivity, $\mathbf{J}$ [LT^{-1}] the water flux, and l_e [L] a characteristic length of the two adjacent elements. On the boundaries, σ reduces to σ_B introduced in Eq. (14), variable which is identical excepted for the l_e parameter which relies on the unique adjacent element.

To increase the stability and efficiency of the model, the mass matrices in Eqs. (22) and (23) have been lumped. Following other model designs, the diffusivity tensor $\mathbf{K}$ has been linearized over each element in terms of its nodal values [34,12]. Eqs. (22)–(24) are discretized in time with an explicit Euler scheme. When correctly implemented, explicit schemes can yield a perfect scaling, as shown in [24]. Indeed, their inherent simplicity and the absence of linear system solver limit the communication overhead between processors. The detailed equations are given in Section 3.3.

3.2. Discretization of the surface model

The surface model has been discretized in space with the CVFE method. This method appears to be more stable and efficient than other methods like the continuous or the discontinuous Galerkin discretizations. It is mainly due to the fact that the CVFE method naturally avoids zero or negative depth issues. Indeed, the flux between two nodes of an element is set to zero if no water is present in the upwind node. Linear and non-linear solvers achieve a better convergence with the CVFE method because the equation coefficients are then constrained to physical values. This allows the use of larger time steps and thus improves of the overall computational speed.

The CVFE method is based on a continuous Galerkin formulation. The expansion of the model unknowns is similar to Eq. (19) with the exception that the basis functions $\phi_i (1 \leqslant i \leqslant n)$ are now piecewise continuous. By applying the classical continuous Galerkin method to Eq. (9), we obtain the following discrete equations:

$$\mathbb{M}\frac{dH}{dt} = NH + B, \tag{36}$$

where $N_{ij}^e = \langle n\nabla\phi_i\cdot\nabla\phi_j\rangle$, $B_i^e = \langle n\nabla b\cdot\nabla\phi_i + q_s\phi_i\rangle$, $n = h^{3/2}\sqrt{g/G}\Big/\sqrt{|\nabla(h+b)|}$ and $\mathbb{M}_{ij}^e = \langle\phi_i\phi_j\rangle$.

To obtain a CVFE discretization, the mass matrix $\mathbb{M}$ is lumped and an inter element upwinding is applied. This amounts to modify diffusive terms in $NH + B$ as follows:

$$\langle n\nabla(u)\cdot\nabla\phi_i\rangle \to n_j(u_j - u_i)\langle\nabla\phi_j\cdot\nabla\phi_i\rangle, \tag{37}$$

where $u = b + h$ and

$$n_j = \begin{cases} n(x_i) & \text{if } (u_j - u_i)\langle\nabla\phi_j\cdot\nabla\phi_i\rangle < 0, \\ n(x_j) & \text{if } (u_j - u_i)\langle\nabla\phi_j\cdot\nabla\phi_i\rangle > 0, \end{cases} \tag{38}$$

When a mesh element is anisotropic, this method can result in negative influence coefficients, *i.e.* $\langle\nabla\phi\cdot\nabla\phi_i\rangle < 0$ [9]. The resulting flux between two nodes is then non-physical, as it follows the pressure gradient instead of being opposite to it. As n is a non-linear function of h, such a flux between two nodes can dominate the other internode fluxes inside the element. The resulting flow inside the element is then unphysical. To avoid those issues the simple solution used here (called approximate CVFE method thereafter) consists in canceling all the negative coefficients:

$$n_j^* \simeq \max(n_j, 0) \tag{39}$$

This approximate CVFE method has only a slight impact on the model solution as compared to the original CVFE, except for anisotropic elements for which the solution is improved (see Section 4.3.1). Since triangular elements are less likely to yield negative influence coefficients than quadrangles, the approximate CVFE method is mainly used for the latter.

Eq. (36) is discretized in time with an implicit Euler scheme. The non-linear solver is based on the Newton–Raphson method and the linear solver is based on the Generalized Minimal RESidual (GMRES) method [35]. The fully discretized equation is given in Section 3.3.

3.3. Summary of the numerical solution procedure

The overall solution procedure for the coupled model is summarized below. For a given parametrization, an initial state (Ψ^0, Θ^0, H^0) and a time step Δt, we iterate over the following steps:

1. Solve the equation for the intermediate steps $\Psi^{n+1,k}$, given $\Psi^{n+1,0} = \Psi^n$:

$$\text{for } k = 1,\ldots,m: \tag{40}$$

$$F_{BC}^k = \text{couple}(H^n, \Psi^{n+1,k-1}) \tag{41}$$

$$\widetilde{C}M\frac{\Psi^* - \Psi^{n+1,k-1}}{\Delta t/m} = K\Psi^{n+1,k-1} - Z + P, \tag{42}$$

$$\Psi^{n+1,k} = \text{limit}(\Psi^*), \tag{43}$$

where m [–] is the number of iterations for the ψ-form, the coupling function is either Eq. (12) or Eq. (14) and the limiter is described in [24].

2. Solve the equation for $\Theta^{n+1,0}$, given Θ^n and $\Psi^{n+1,m}$:

$$F_{BC} = \text{couple}(H^n, \Psi^{n+1,m}) \tag{44}$$

$$M\frac{\Theta^* - \Theta^n}{\Delta t} = K\Psi^{n+1,m} - Z + P, \tag{45}$$

$$\Theta^{n+1,0} = \text{limit}(\Theta^*). \tag{46}$$

3. Compute Ψ^{n+1} by combining $\Psi^{n+1,m}$ and the retention curve relationship:

$$\Psi^{n+1} = \begin{cases} f_\theta^{-1}(\Theta^{n+1,0}) & \text{in the dry zone,} \\ \Psi^{n+1,m} & \text{in the wet and the saturated zones.} \end{cases} \tag{47}$$

4. Weakly correct $\Theta^{n+1,0}$ in the wet and the saturated zones:

$$\text{for} k = 1,\ldots,q: \tag{48}$$

$$M\frac{\Theta^{n+1,k} - \Theta^{n+1,k-1}}{\Delta t} = \Lambda(\Theta^{n+1,k-1} - f_\theta(\Psi^{n+1})) + P^\theta, \tag{49}$$

where q [–] is the number of iterations for the θ filter and where $\tilde{\Psi}$ is defined as Ψ^{n+1}.

5. Implicitly solve the equation for H^{n+1} using F_{BC}:

$$\mathbb{M}\frac{H^{n+1} - H^n}{\Delta t} = NH^{n+1} + B^{n+1} + P_h^{n+1}, \tag{50}$$

In the current form of the model, the parameters m and q are set manually based on indicators of convergence like an excess of water content. Indeed, a bad convergence in saturated areas creates non-elliptical fluxes that yields a unphysical water content above the saturation limit. A method to estimate those two parameters along with the time step in order to optimize the computation time is still needed to obtain a model suitable for long-term simulations.

4. Results

This section is divided into four subsections presenting different test-cases that highlight the model properties. First, we verify the ability of the surface model and of the coupled model to reproduce results of similar models in three test-cases. Then a well-known integrated modeling example from a field-scale experiment is given. A third section analyses the sensitivity of two aspects of the presented model: the anisotropy of surface elements and the FOEC coupling. Finally, results for both strong and weak scalings are presented.

As the whole model is mass conservative at machine precision and as the 'double' C++ floating number precision has been used, the relative mass balance error for all the simulations stays below 10^{-15}.

4.1. Model verification and validation

The model verification is done through the validation of the two sub-models and the validation of their coupling. The subsurface model has been validated in a previous publication [24]. The surface model implementation with the CVFE method is compared with the tilted V-catchment 2D example from [8] that has been extensively used to validate surface models (as for instance [7,36]). As this method has already been proved accurate [8,9,12,11], we only assess the reproducibility of the results with our implementation.

The hybrid coupling method is used in the two coupled test cases of this section. The coupled model is firstly validated with a test case of Kollet and Maxwell [18] to check the model's ability to handle an Hortonian runoff process. The second validation case is the sandbox example of Abdul and Gillham [37] which is based on experimental outflow results and has been extensively simulated [38,18,7,36]. It presents both infiltration and exfiltration and is especially challenging for the subsurface model as the almost totally saturated media loads to for a strong elliptical behavior. Similar results with some PC coupling models can assess for a fast-enough convergence of the coupling methods towards the PC coupling.

4.1.1. Surface model – impermeable V-catchment

The numerical setup of [8] consists in a impermeable 1000×800 m plane, with a slope of 2% along its length and 5% along its width. A 1-m deep and 10-m wide channel is located at the bottom and carries the water towards the unique outlet of the domain. The Manning roughness coefficient is set to 0.015 s $m^{-1/3}$ for the plane and 0.15 s $m^{-1/3}$ for the channel. Zero-flux boundary conditions are imposed everywhere except at the outlet of the channel where a critical depth boundary condition is used. The initial state is a dry surface. A uniform and constant rain is then applied for 90 min with a rate of 3×10^{-6} m/s. The resulting outflow, computed on a regular mesh of 100-m resolution squares and a time step of 100 s, is shown in Fig. 1. The other model results were obtained with a 100-m resolution and time steps ranging between 5 and 600 s. It can be seen that our model produces an hydrograph very close to the ones obtained with HGS which also uses the CVFE method, SHE [8] or MODFLOW-SURFACT. The results of di Giammarco [8] (CVFE and finite differences) converge more quickly to the steady state. This delay can be reduced by refining both the temporal and the spatial

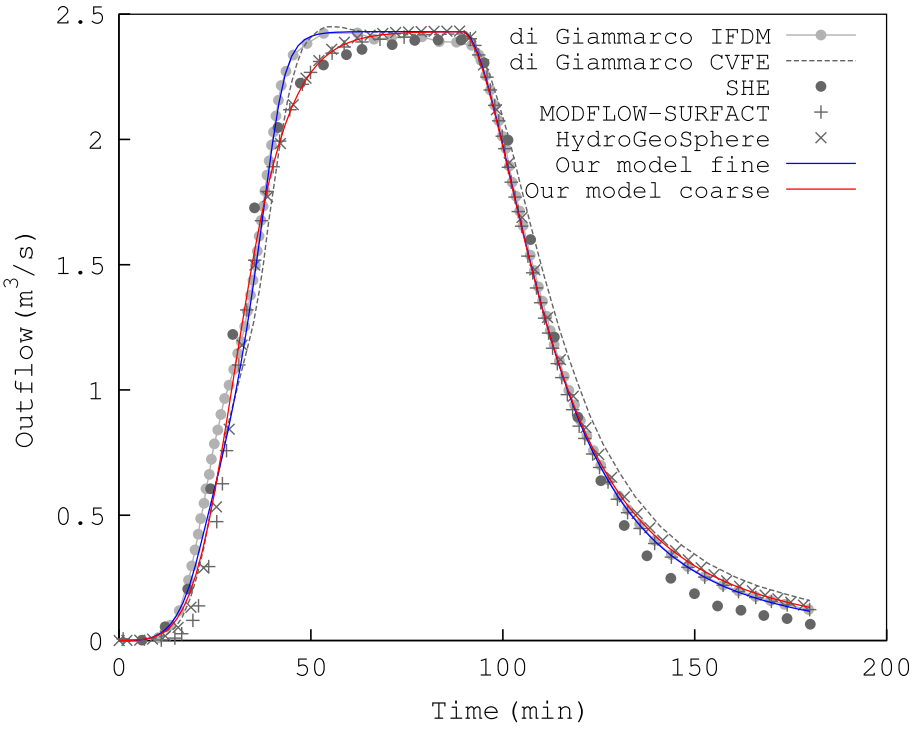

Fig. 1. The V-catchment test case assesses the ability of a model to handle the simplest valley-shaped geometry. The outflow of our model is within the range of other model outflows presented in [9,12]. The fine/coarse discretizations are of 10/100 m in space and 1/100 s in time.

discretization as can be seen for the simulation with finer resolutions of 10 m and 1 s in Fig. 1.

4.1.2. Coupled model – Hortonian runoff

Kollet and Maxwell (K&M) [18] present several modeling examples that focus on the surface–subsurface coupling. Their runoff production by excess infiltration test case (Hortonian runoff) consists in a 1D surface slope of 0.0005 spread over 400 m and characterized by a Manning coefficient $n = 0.019872\ \mathrm{s\,m^{-1/3}}$. The underlying soil is uniform and is characterized by $\theta_s = 0.4,\ \theta_r = 0.08,\ \alpha = 1,\ \beta = 2$. The parameter K_s is set either to 1.1574×10^{-7} or 1.1574×10^{-6} m/s, to assess two different behaviors. The initial water depth is set to 1 m below the surface. A rain of 5.5×10^{-6} m/s is applied during 200 min. We kept the same discretization as K&M, which is of 80 m along the slope and either 1 or 5 cm vertically.

An analytical solution of this problem exists but only for an impermeable slope. In order to use that solution, we therefore perform simulations without any infiltration. The resulting hydrograph is provided as a reference as it represents the situation without infiltration [31]. Our model reproduces accurately the beginning of the event and the beginning of the recession, with a discrepency before reaching the steady state (see Fig. 2). With the same discretization, our surface model has the same accuracy as the model of K&M. K&M showed that the analytical profile can be approached with refinement of the spatial resolution [18].

We then consider the case with the lower soil conductivity (Fig. 3), for which most of the rain input leaves the domain without infiltrating in the soil. When spatial and temporal discretization are refined, our model converges towards a slightly different solution than K&M, which can be explained by the different coupling approaches. The value of α_{FOEC} chosen by K&M is not specified but it is expected to be smaller than our value of σ_B in the 1 cm case and larger in the 5 cm case. Indeed, the infiltration is less important in their 1 cm case, due to a weaker coupling. The opposite can be seen for the 5 cm case. This is seemingly due to the use of a similar value of α_{FOEC} for both their 1 cm and 5 cm cases, resulting in different fluxes (see Section 4.3.2 for details). Our model is less sensitive to a coarser spatial discretization, as the σ_B adapts itself to the subsurface element size. The coarse temporal resolution of 180 s is less appropriate for our explicit subsurface model, but it can still be handled with additional sub-iterations ($q = 10, m = 2$).

The case with the higher soil conductivity is shown in Fig. 4. A space–time resolution of 1 cm/180 s has proved to be too coarse in time for the explicit solver. We found that a 1 cm/10 s resolution was required, which increased the number of sub-iterations to $q = 10$ and $m = 2$. Our model is in good agreement with the K&M one, except at the end of the simulations where a change of regime occurs. This is due to a complete saturation of the soil, which means that runoff is non-Hortonian at the end of the simulation. The soil pressure head has therefore to switch from an infiltration profile to an incompressible groundwater profile, which are very different. The explicit model needs extra iterations when this abrupt change occurs, to produce the same results in the 5 cm cases. The discretization of 1 cm was too fine to converge towards this regime change with a reasonable number of iterations. It can be seen again that our model is less sensitive to the coarser discretization than the K&M model, seemingly for the same reasons as above.

4.1.3. Coupled model – Sandbox

Abdul and Gillham [37] have studied the effect of the capillary fringes over the overland flow generation. The model domain consists in the sandbox shown in Fig. 5 with its related parameters. The geometry allows the use of a 2D model for subsurface flow and 1D model for surface flow. The water table is initially at a steady state and at the same height as the outlet located at the bottom of the surface slope. A rainfall is applied uniformly for 20 min at a constant rate of 4.3 cm/h. The discharge is monitored from the beginning of the rainfall to almost the end of the recession period.

The 2D mesh is unstructured and made of 252 triangles with a higher resolution near the surface. The characteristic lengths of the elements goes from 2.4 to 25.1 cm. The 1D surface model is discretized according to the topmost segments of the 2D mesh. A

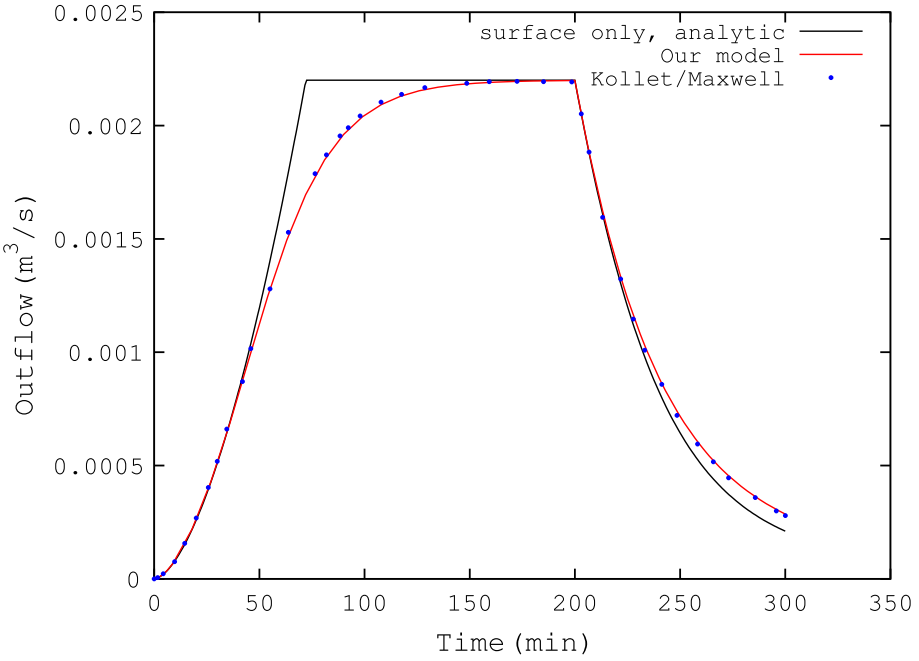

Fig. 2. Analytical solution of a rain outflow over a simple impermeable slope and its resolution by our model and the Kollet & Maxwell model. The models results use coarse time and space discretization (180 s, 80 m), which can explain the divergence from the analytical solution.

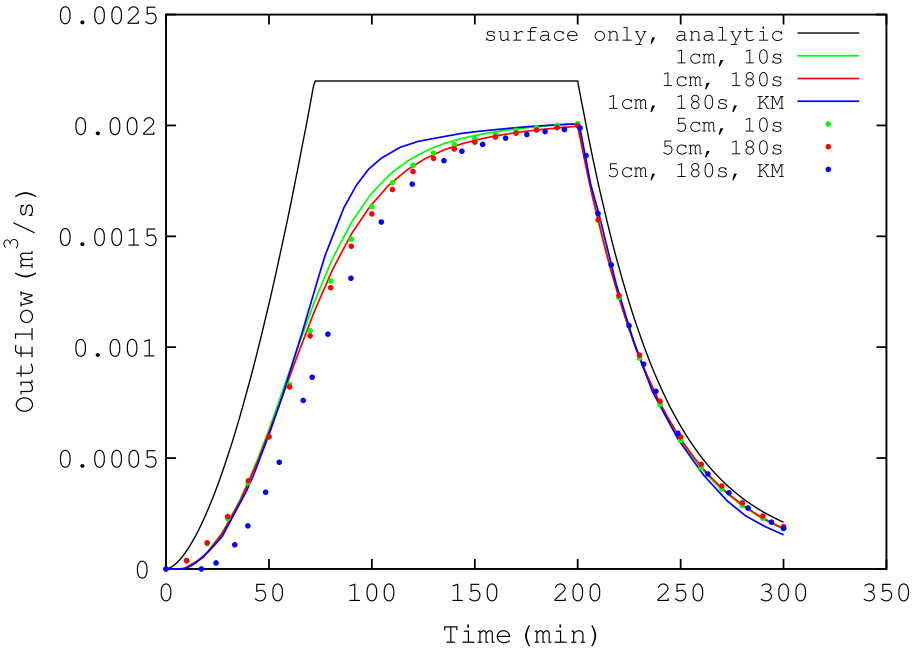

Fig. 3. Outflow for a simple slope over homogeneous soil with $K_s = 1.1574 \times 10^{-7}$ m/s. The results obtained by K&M [18] are shown in blue. The other results are from our model. In those runs, q and m are kept to 1 excepted for the 1 cm/180 s case which needed more convergence with $q = 10$ and $m = 2$. It can be seen that our model converges towards a slightly different solution than the K&M one as the spatial or temporal resolutions are refined. Our results are less influenced by the coarser spatial resolution. The analytical solution of Fig. 2 is kept for comparison. (For interpretation of the references to color in this figure legend, the reader is referred to the web version of this article.)

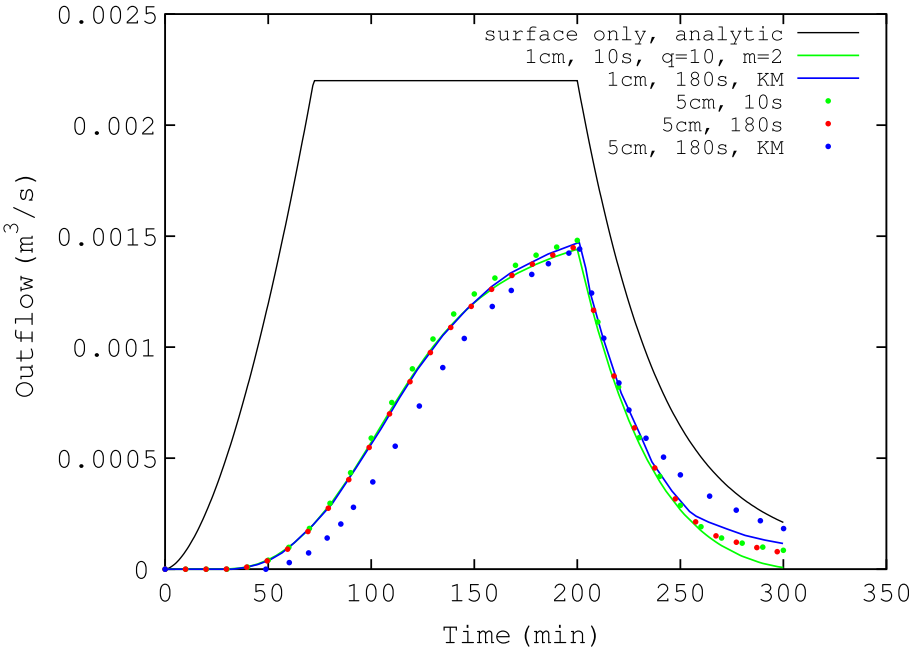

Fig. 4. Outflow for a simple slope over homogeneous soil with $K_s = 1.1574 \times 10^{-6}$ m/s. The results obtained by K&M [18] are shown in blue. The other results are from our model. The q and m for the 5 cm/10 s and 5 cm/180s cases are 1 excepted between 258 and 267 min where they were manually set to 100 to achieve convergence. Our model results are close to the fine-resolution result of K&M, even for the coarser resolution. The analytical solution of Fig. 2 is kept for comparison. (For interpretation of the references to color in this figure legend, the reader is referred to the web version of this article.)

constant time step of 0.1 s is used. The beginning of the simulation requires an increased number of iterations for ψ, so m is manually set to 100. After 200 s, m is set to 10. During the whole simulation, the maximum number of iterations for the filter q is set to 4.

Different models are presented for comparison in Fig. 6. The temporal and spatial discretizations are of 10 s and 1×4 cm quadrilaterals for ISWGM [36], of 0.1–10 s and 2×2.8 cm quadrilaterals for Cast3M [7], of 10 s and 1×2 cm quadrilaterals for Parflow [18] and of 60 s (max) and 2 cm sided squares for InHM [9]. Fig. 6 shows that our model is consistent with experimental data and other published models results. The origin of the discrepancy between the models results is difficult to assess as the model resolutions are different. It should be noted that all models reach a steady state slightly ahead of the real system. K&M suggested that this is due to the presence of air phase compression in the experiment [18]. As the simulated flow

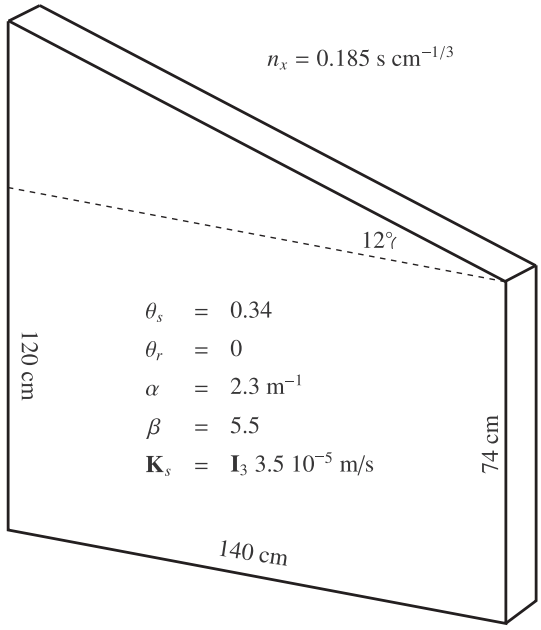

Fig. 5. Geometry and physical properties of the sandbox test case. A uniform rainfall is applied on the top and the unique outlet is situated at the top right corner of the domain.

profile is very similar to those already published, it is not shown here.

4.2. Integrated 3D modeling example

A field-scale experiment has been performed by Abdul [39] in a small catchment of the Canadian Forces Base Borden, Ontario, Canada. The area of 1070 m^2 is grass covered except for a channel approximately 60 cm wide, located 22 cm below the streambed. The sandy soil is characterized by the following parameters: $\theta_s = 0.34$, $\theta_r = 0.0612$, $\alpha = 6\ \text{m}^{-1}$, $\beta = 1.9$. $\mathbf{K}_s$ has an isotropic value of 10^{-5} m/s. The initial water table is at a depth of 20 cm below the channel.

The 3D mesh is constituted of triangular prisms vertically extruded over 6 layers from the 2651 triangles that constitute the surface mesh, for a total of 95.436 subsurface DOF's (see Fig. 7). The surface mesh is refined in and near the channel while the subsurface mesh is refined near the soil surface. The time step is set to 5 s. The parameters m and q that specify the number of iterations are set to 4 and 1, respectively. A uniform rain of 5.55×10^{-6} m/s is applied during 50 min.

Most of the surface-subsurface models use this test case as a benchmark. The four we are showing use finite difference (MODFLOW) or CVFE (Groundwater, Hydrogeosphere and Vanderkwaak) schemes in space and Euler implicit schemes in time. They are all using the non-inertia approximation of the shallow water equations. The spatial mesh of the surface is the same for all models. The vertical resolution at the surface is coarser in our case: 10 cm compared to 1 cm, which leads to 15 layers for the other models.

In this test case, the FOEC coupling described by Eq. (12) is used. Indeed, it appeared that the hybrid coupling underestimated the surface flux, as most of the rain infiltrates. This is the physical behavior with the present parametrization for a dry soil, as the rain flux is below the saturated conductivity. Therefore the rain has to infiltrate until non-Hortonian overland flow occurs. As experimental data show a non-negligible amount of surface water, we deduce that something slows down the infiltration. It may be the vegetation or some surface compaction of the soil. We therefore had to calibrate the model outflow with a specific value of α_{FOEC}, as suggested by Ebel et al. [27]. Manual calibration leads us to take $\alpha_{FOEC} = 0.25\ \text{s}^{-1}$. This value is around $0.1\ \text{s}^{-1}$ for InHM [9], and $10^{-4}\ \text{s}^{-1}$ for GroundWater and Hydrogeosphere [11,12]. Despite the coarser vertical resolution, the hydrograph obtained with our model is close to observed and modeled values (see Fig. 8).

The origin of the early delay between most of the simulated results and the observations is difficult to assess. A possible explanation is that a local surface storage is present and has to be filled before any outflow can occur, or that the initial rain is overestimated. Both cases can delay the measures. Another possible explanation is that the runoff is non-Hortonian. In this case, it possible that the initial water table depth is above the specified value, or that the subsurface water is not at equilibrium and more water

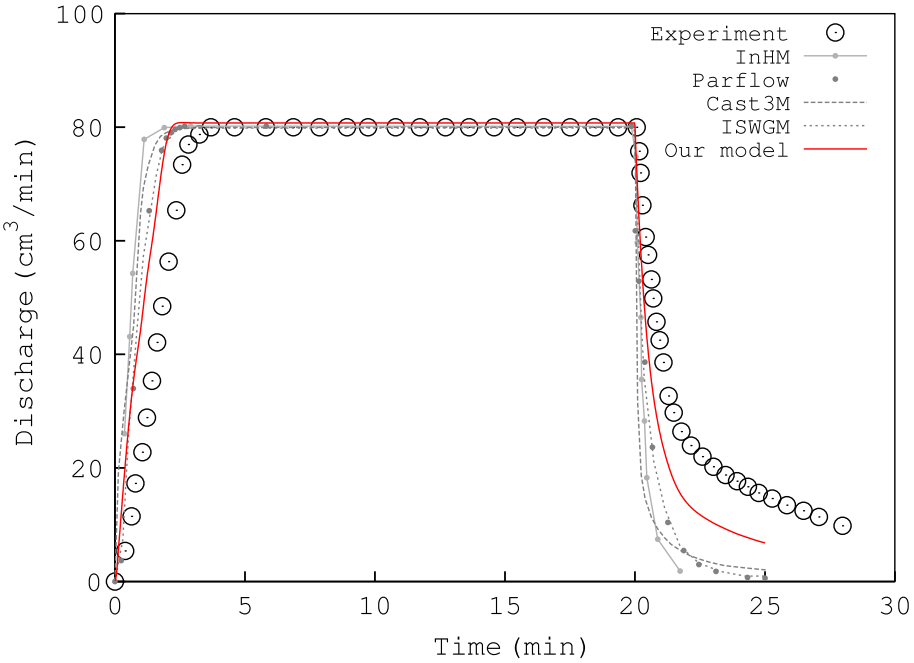

Fig. 6. Derived and simulated hydrographs of the sandbox test case and our model results are in good agreement with observed data.

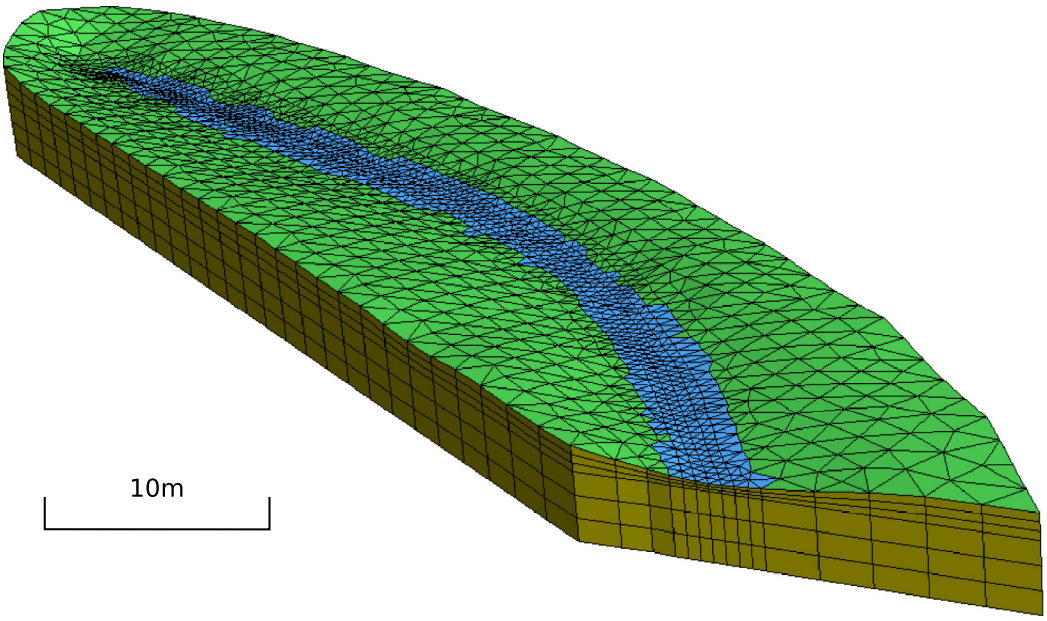

Fig. 7. The 3D mesh used for the Borden test case. The channel is displayed in blue, grass land in green and the subsurface part in brown. The surface mesh is refined inside the channel. The first three of the six vertical layers are refined to represent the larger fluctuations present in the unsaturated zone. (For interpretation of the references to color in this figure legend, the reader is referred to the web version of this article.)

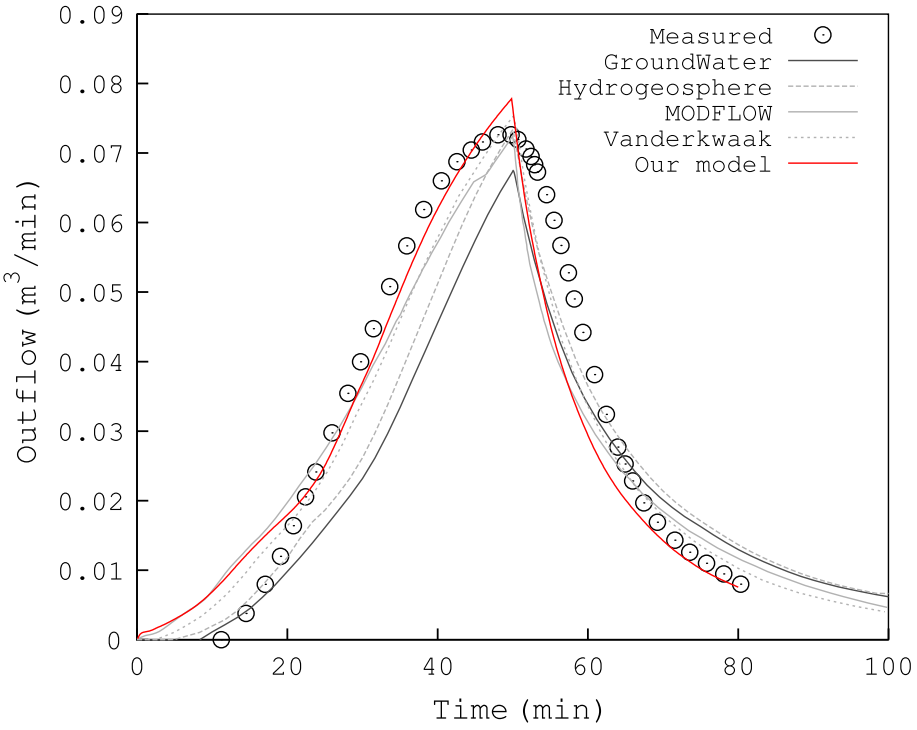

Fig. 8. Hydrographs obtained after a 50 min rainfall event over the Borden catchment. Our model results are in good agreement with observed values and other state-of-the-art models.

is present in the unsaturated area [10], or that the rain is underestimated. In such cases, it is possible to reach a non-Hortonian runoff with the hybrid coupling earlier in the simulation and hence explain the absence of outflow during the infiltration.

4.3. Sensitivity analysis

Two issues were experienced during the model implementation. Both were linked to the spatial discretization. The first one is related to the CVFE method used for the surface model that is not well suited to anisotropic elements. The second one concerns the FOEC method used to add extra physics at the soil-surface interface that is strongly dependent of the subsurface discretization. In this section, we describe those issues and present the solutions that we implemented in our model.

4.3.1. Surface model – anisotropic elements

The above V-catchment test case produce unphysical results when the CVFE method is applied with a coarse discretization of quadrangles. We have therefore studied the effect of different

mesh resolutions on the model results. The time discretization error is negligible as the time step is set to 1 s.

When the mesh resolution is larger than 10 m, we have to use rectangular elements in order to still be able to represent the 10 m wide channel of the V-catchment. The anisotropy of the mesh elements and the non-linearity of the equations can produce unphysical fluxes going in the wrong direction if the influence coefficient method is not modified. Fig. 9 shows that for the 40 m discretization the approximate CVFE method keeps a correct value for the discharge when the mesh is coarsened, which is not the case with the original CVFE method. This is highlighted for the 100 m discretization, where the result is just slightly different with the modified method, but totally wrong with the classical method for which unphysical fluxes are clearly visible in the channel (not shown). The results – with and without the approximation – for the mesh with a discretization of 10 m are not differentiable graphically as the mesh is entirely made of square elements (*i.e.* isotropic) and can therefore not produce negative coefficients.

4.3.2. Coupled model – effect of the parameter α_{FOEC}

It has been observed in the Borden test case that the first layers of the subsurface discretization have a large influence on the infiltration. To highlight this aspect of the FOEC coupling, a 1D vertical example has been considered, where the surface water can only flow in the soil or accumulate. The same properties as in the Borden test case are used, *i.e.* the depth, rain and initial conditions correspond to the ones of a column in the middle of the 3D channel. A uniform vertical discretization is used with different resolutions ranging from 1 cm to 80 cm. The surface water depth is monitored during 75 min (see Fig. 10). When refining the subsurface discretization and keeping α_{FOEC} constant, infiltration decreases, and the surface water depth thus increases. This effect vanishes when the grid size reaches 5 cm and the infiltration front is sufficiently resolved. However, the use of a large vertical discretization is desirable for large-scale and/or long term studies. One simple explanation to the phenomenon is that large subsurface elements have a larger storage capacities. They are therefore less sensitive to a given influx than smaller ones. The coupling flux based on a nearly constant value of the pressure head is also nearly constant, and therefore remains important. To circumvent this issue it is possible to increase the value of α_{FOEC} and to use it as a fitting parameter like in the Borden test-case. Its optimal value is then obviously problem and mesh-dependent.

Effects of the near-surface vertical resolution on the results have already been discussed for subsurface models. It has been observed in the case of a 2D groundwater finite volume model that the vertical discretization highly affects the results [40]. Downer and Ogden [41] point out the necessity to use fine vertical discretization at soil surface (~1 cm) in a finite difference model with a Dirichlet (when ponding) or Neumann (when dry surface) boundary condition coupling. They showed in particular that the amount of infiltration is highly dependent on the element size. It increases as the grid size decreases. They highlight the importance of the evaluation of K in their coupling. Indeed as the value of K in initially dry soil is very low, classical boundary fluxes relying on local K values are strongly under-estimated. Their observations are however not relevant to our issues as in our case the amount of infiltration *decreases* as the grid size decreases. We already circumvented their issue by taking the upwind value of K in interface fluxes. This means that $K = K_s$ at the surface when infiltration occurs and the surface is thus considered as either fully saturated or dry.

4.4. Model efficiency

The model efficiency with the hybrid coupling is assessed based on strong and weak scaling test cases. The former highlight the ability of a model to use small computational domains per nodes, which lead to an increasing domain surface/domain volume ratio. That implies an increase of the intra-nodes communication then a decrease of the scalability. A model still scalable with a large ratio

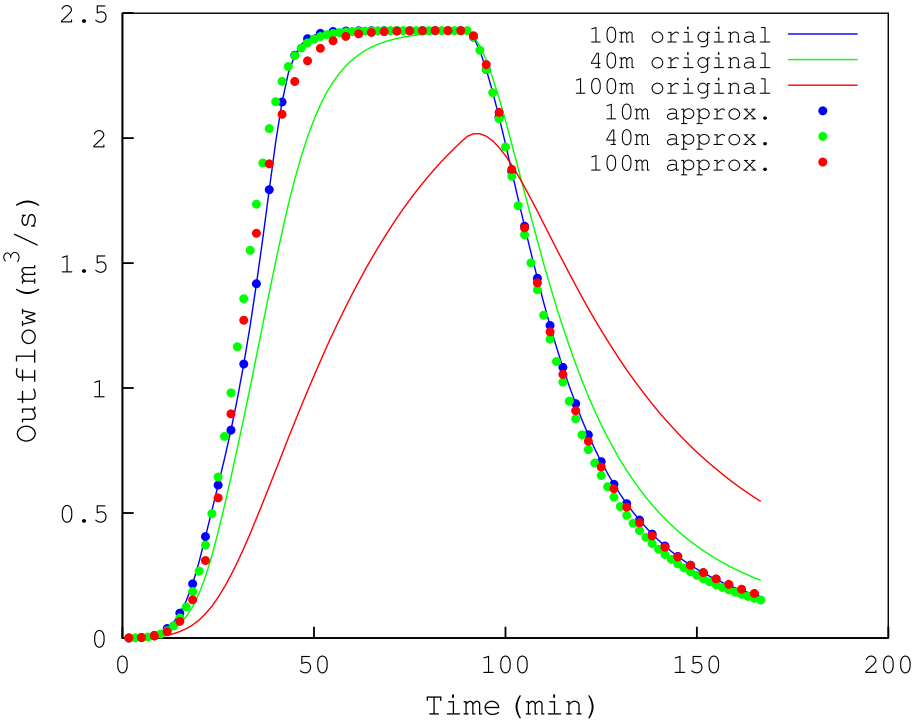

Fig. 9. The outflow of the V-catchment experiment is greatly influenced by anisotropic elements when using the original CVFE method. The proposed approximation, in which the negative influence coefficients are set to zero (*i.e.* only positive coefficient are kept), greatly improves the results on coarser meshes as compared to the original CVFE formulation.

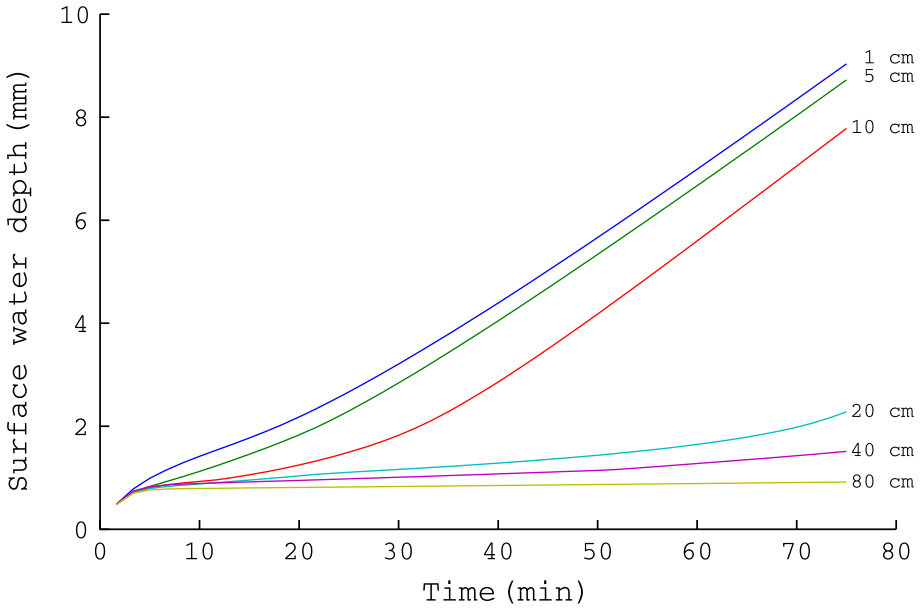

Fig. 10. The surface water height obtained with a single 1D infiltration model without surface fluxes strongly depends on the vertical grid resolution. The grid size has to be fine enough to capture the infiltration front otherwise the $h-\psi$ difference thus the coupling flux stay important.

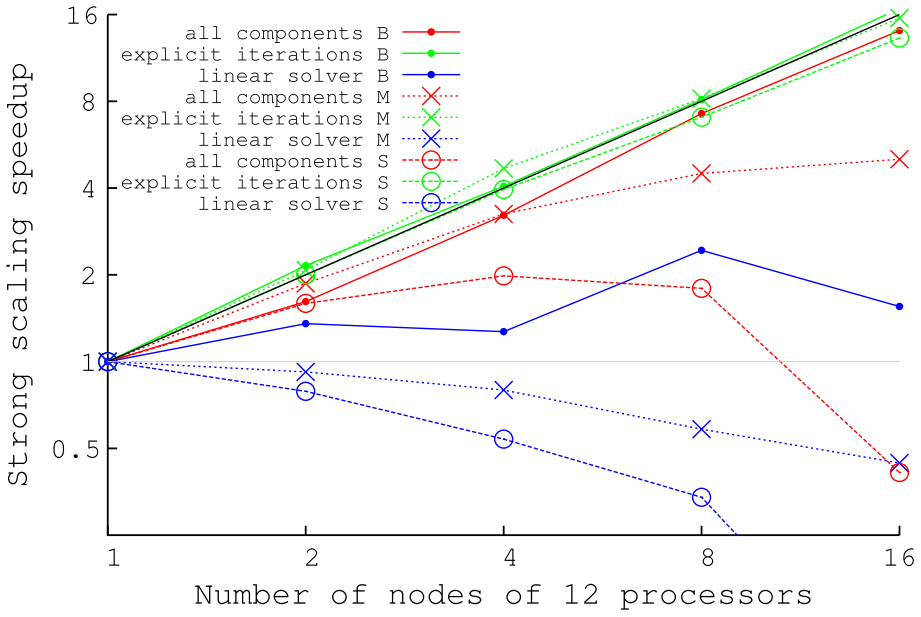

Fig. 11. The black line represents an optimal strong scaling, *i.e.* doubling the computational power doubles the speed. The letters are for the small mesh (S), the medium mesh (M) and the big mesh (B). Two components of the model are highlighted: the explicit iterations from the subsurface model and the linear solver from the surface model. The model strong scaling is optimal for the explicit discretization of the Richards' equation, but not for the implicit discretization of the non-inertia shallow water equation, as expected. The latter reduces the scaling of the overall model but can handle much bigger time steps than an explicit discretization of the non-inertia equation.

has a good strong scalability. The latter is used to assess the capacity of a model to extend its computational domain still keeping a good scalability. This is certainly a good property for large-scale simulations.

4.4.1. Strong scaling

The first 50 s of the Borden test case where taken as benchmark to assess the model strong scaling. For those computations, two additional meshes of 4.48×10^5 and 1.37×10^7 DOF's have been used. With 192 processors, the load per processor is then of 497 DOF's for the mesh previously used and respectively of 2.9×10^3 and 7.15×10^4 DOF's for the two larger ones. The 6 layers of depth were kept, leading to a subsurface/surface DOF number ratio of 7. To limit the side effect of memory-sharing between the processors of a same node, we set a whole node of 12 processors as the reference. The partitioning of the whole domain into sub-domains has been done for the surface model. This sub-domain and the soil column under it are associated to a unique processor core.

The results in Fig. 11 show a good scaling for the larger problem, a correct one for the medium problem and a poor scaling for the small problem. The identification of the scaling performance for the different parts of the algorithm highlights the source of the poor scaling. Although the solution of subsurface model is the most expensive, it scales optimally as shown in [24]. However, the surface part relies on an implicit solver which requires many inter-

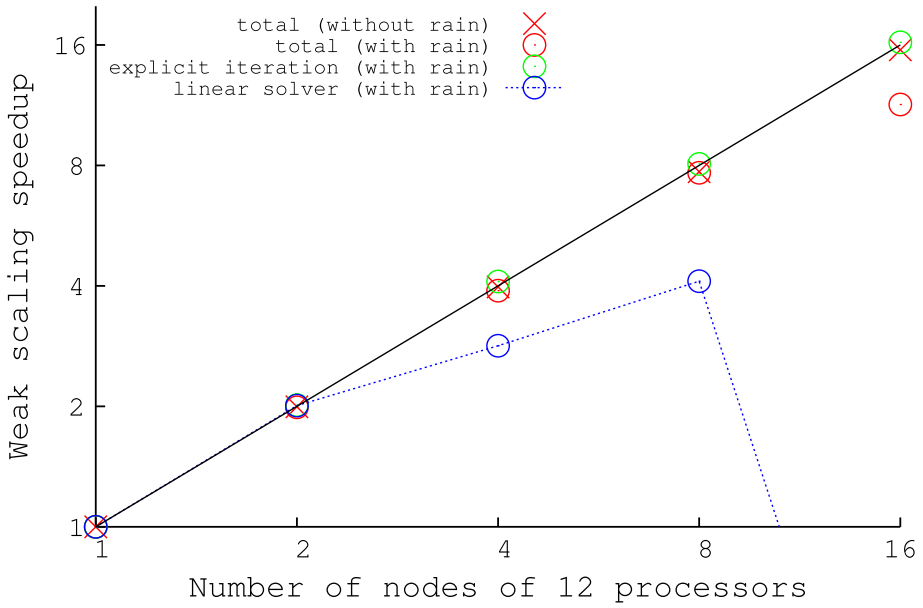

Fig. 12. Weak scaling of the model over up to $16 \times 12 = 192$ processors. The black line represents an optimal weak scaling. In the absence of a surface flow, the model weak scaling is optimal as expected from the explicit time discretization of the subsurface model. When there is a surface flow, the model overall scaling is impacted by the suboptimal scaling of the linear solver used for the implicit time discretization of the surface model. The poor scaling of the surface model is particularly clear when more than 96 processors are used.

processor communications, especially when the surface water is at rest. Therefore the scaling of the surface model decreases when to the number of DOF's per processor goes down. The summation of these two effects does not preclude an overall good scaling, as long as the load associated with the surface model is below the load of the subsurface model, which is one order of magnitude larger on one processor in this test case.

4.4.2. Weak scaling

The weak scaling is interesting as it does not benefit from the extra resources coming from the additional nodes, as each new node has to handle the same computational burden as the others. The scaling is then restricted to a maximum of 100%. Obtaining a good weak scaling is often sufficient for fine resolution and/or large scale applications that allocate a large sub-domain per processor. Maxwell [19] has presented a non-dimensional test case optimized for weak scaling. It consists in a sinusoidaly-shaped layer of homogeneous soil. We slightly differ from this test case by considering that $\tan(x) \simeq x$ when x is close to zero, resulting in the topography formula $z = \sin(x/5)/2 - \cos(y/5)/2$. The problem size per processor is decreased from a 100×100 to a 50×50 square, with a constant depth of 25. The regular mesh is composed of hexahedrons with 2×2 horizontal sides and a depth of 1. In this test case, all quantities are dimensionless. The number of DOF's per processor has then been decreased from 5×10^5 to 1.25×10^5.

The soil properties are set to $\mathbf{K} = 0.25 \times \mathbf{I}_3$, $\theta_s = 0.25$, $\theta_r = 0.025$, $\alpha = 1$ and $\beta = 3$. The initial ψ is set to -10 at the ground surface, hydrostatic equilibrium being imposed vertically *i.e.* the water table is following the topography, and is then initially out of equilibrium. No rain is applied, which means that the surface domain remains completely dry. The duration of the simulation is set to 10 with a time step of 2.

Fig. 12 shows the weak scaling result for this test case. Our model exhibits a nearly-optimal weak scaling. The negative effect of the surface model on the scaling is absent as its solution is trivial when the surface is dry. As this test does not show the ability of the whole coupled model to achieve a good weak scaling, we have added a homogeneous time-dependent rainfall $r(t) = 0.2 + 0.01t$, which triggers a surface flow. The resulting scaling is depicted in Fig. 12, and like with the strong scaling test case, the weak scaling of the coupled model is negatively impacted by the surface model.

5. Conclusion

In this study, we have presented a new coupled model for the surface–subsurface water interaction. The subsurface flow is described by the Richards' equation, which has been discretized in time with an Euler explicit scheme and in space with a first-order DG FE scheme. The surface flow is described by the non-inertia approximation of the shallow water equations. It is discretized with an implicit scheme in time and a control volume finite element scheme in space. Both models are coupled by weakly imposing the continuity between surface and subsurface pressures.

The CVFE method is well designed for the non-inertia shallow water equation as it naturally handles the zero-depth issue. However, the influence coefficients of this method can become negative for anisotropic elements. Negative coefficients lead to unphysical fluxes between mesh nodes, which can severely impair the model accuracy if left unchecked. We have shown that by simply setting negative coefficients to zero we can avoid that issue.

The proposed coupling lies between the pressure continuity coupling and the FOEC coupling methods. Indeed, it uses both a weak imposition of the continuity between the surface hydrostatic pressure and the subsurface pressure head, improving the scheme robustness, and it reduces to the pressure continuity coupling when the surface and subsurface pressures have converged. The FOEC can be used to add sub-scale surface–subsurface interactions as a slower interface conductivity, which is not the case of our hybrid coupling. However the FOEC flux can be discretization-dependent if the infiltration front is not fully resolved, which means that it has to be used with caution for coarse vertical discretization, as it is often the case in large-scale and/or long-scale studies. With the hybrid coupling presented in this study, the coefficients are element-size dependent and are coherent with the inter-element treatment of the rest of the subsurface domain. The proposed coupling comes handily along with the DG FE discretization without

having to fix a free parameter value, and seems more robust for coarser subsurface discretization. This coupling also uses a unique time step which is designed for both surface and subsurface models. Indeed, an explicit scheme is well suited to the slow dynamics of the subsurface flow, while the fast surface flow requires an implicit solver. By coupling then two sub-models together, we can use a unique nearly-optimal time step for the global model.

The explicit discretization of the Richards' equation leads to a perfect strong scaling. The surface model being implicit, it cannot achieve the same optimal scaling as the subsurface model. However, as the computational load of the non-inertia equation is generally one order of magnitude smaller than the load of the Richards' equation, the negative influence of the implicit scheme on the overall scaling remains limited. As a result, the proposed coupled model shows both good weak and strong scalings. We believe that such a modeling approach will prove useful in the future as the current trend in high-performance scientific computing is to favor large scale parallel architectures that require scalable models. However, to become an operational large-scale and long-term model, several improvements are still mandatory. First, an purely elliptic solver should be used in the saturated areas, such as the multi-grid method. That would slightly degrade the scaling, but it is necessary to handle large aquifers. Secondly, an adaptive time stepping scheme which also adapts the number of sub-iterations is required to automatically optimize the performances over time, while keeping a specified accuracy. Eventually, evapotranspiration will have to be taken into account for long term studies, as it is a key component of the terrestrial water cycle.

Acknowledgements

Thomas De Maet is a research fellow with the *Fonds spécial de recherche* (FSR) of the *Université catholique de Louvain*. The present study was carried out in the framework of the project *Taking up the challenges of multi-scale marine modeling*, which is funded by the Communauté Française de Belgique under Contract ARC 10/15-028 (Actions de Recherche Concertées). Computational resources have been provided by the supercomputing facilities of the Université catholique de Louvain (CISM/UCL) and the Consortium des Equipements de Calcul Intensif en Fédération Wallonie Bruxelles (CECI) funded by the Fond de la Recherche Scientifique de Belgique (FRS-FNRS).

References

[1] Paniconi C, Wood E. A detailed model for simulation of catchment scale subsurface hydrologic processes. Water Resour Res 1993;29(6):1601–20.
[2] Salvucci G, Entekhabi D. Hillslope and climatic controls on hydrologic fluxes. Water Resour Res 1995;31(7):1725–39.
[3] Beven K. Rainfall–runoff modelling: the primer. John Wiley and Sons; 2011.
[4] Liu Z, Todini E. Towards a comprehensive physically-based rainfall–runoff model. Hydrol Earth Syst Sci 1999;6(5):859–81.
[5] Camporese M, Paniconi C, Putti M, Orlandini S. Surface–subsurface flow modeling with path-based runoff routing, boundary condition-based coupling, and assimilation of multisource observation data. Water Resour Res 2010;46(2):W02512.
[6] Santillana M, Dawson C. A local discontinuous Galerkin method for a doubly nonlinear diffusion equation arising in shallow water modeling. Comput Methods Appl Mech Eng 2010;199(23–24):1424–36.
[7] Weill S, Mouche E, Patin J. A generalized Richards equation for surface/subsurface flow modelling. J Hydrol 2009;366(1–4):9–20.
[8] Giammarco PD, Todini E, Lamberti P. A conservative finite elements approach to overland flow: the control volume finite element formulation. J Hydrol 1996;175(1):267–91.
[9] VanderKwaak J. Numerical simulation of flow and chemical transport in integrated surface–subsurface hydrologic systems. Dissert Abstr Int Part B: Sci Eng 2000;60(7):3170.
[10] VanderKwaak J, Loague K. Hydrologic-response simulations for the R-5 catchment with a comprehensive physics-based model. Water Resour Res 2001;37(4):999–1013.
[11] Cornaton F. Ground water manual (version 3.2.9). Switzerland: University of Neuchâtel; 2012. p. 422.
[12] Therrien R, McLaren R, Sudicky E, Panday S. A three-dimensional numerical model describing fully-integrated subsurface and surface flow and solute transport. Tech. rep., Groundwater Simulations Group; 2012.
[13] Celia M, Zarba R, Bouloutas E. A general mass-conservative numerical solution for the unsaturated flow equation. Water Resour Res 1990;26(7):1483–96.
[14] Forsyth P, Wu Y, Pruess K. Robust numerical methods for saturated–unsaturated flow with dry initial conditions in heterogeneous media. Adv Water Resour 1995;18(1):25–38.
[15] Chavent G, Roberts J. A unified physical presentation of mixed, mixed-hybrid finite elements and usual finite differences for the determination of velocities in waterflow problems. Tech. rep., Institut National de Recherche en Informatique et en Automatique; January 1989.
[16] Li H, Farthing M, Dawson C, Miller C. Local discontinuous Galerkin approximations to Richards' equation. Adv Water Resour 2007;30(3):555–75.
[17] Freeze R. Threedimensional, transient, saturated–unsaturated flow in a groundwater basin. Water Resour Res 1971;7(2):347–66.
[18] Kollet S, Maxwell R. Integrated surface–groundwater flow modeling: a free-surface overland flow boundary condition in a parallel groundwater flow model. Adv Water Resour 2006;29(7):945–58.
[19] Maxwell R. A terrain-following grid transform and preconditioner for parallel, large-scale, integrated hydrologic modeling. Adv Water Resour 2012;53:109–17.
[20] Hardelauf H, Javaux M, Herbst M, Gottschalk S, Kasteel R, Vanderborght J, et al. PARSWMS: a parallelized model for simulating three-dimensional water flow and solute transport in variably saturated soils. Vadose Zone J 2007;6(2):255–9.
[21] Herbst M, Gottschalk S. On preconditioning for a parallel solution of the richards equation. Comput Geosci 2008;34(12):1958–63.
[22] Flemisch B, Darcis M, Erbertseder K, Faigle B, Lauser A, Mosthaf K, et al. DuMu^x: DUNE for multi-{phase,component,scale,physics,...} flow and transport in porous media. Adv Water Resour 2011;34(9):1102–12.
[23] Dawson C. A continuous/discontinuous Galerkin framework for modeling coupled subsurface and surface water flow. Comput Geosci 2008;12(4):451–72.
[24] De Maet T, Hanert E, Vanclooster M. A fully-explicit discontinuous Galerkin hydrodynamic model for variably-saturated porous media. J Hydrodyn 2014;26(4):594–607.
[25] Fleckenstein JH, Krause S, Hannah DM, Boano F. Groundwater–surface water interactions: new methods and models to improve understanding of processes and dynamics. Adv Water Resour 2010;33(11):1291–5.
[26] Maxwell RM, Putti M, Meyerhoff S, Delfs J-O, Ferguson IM, Ivanov V, et al. Surface-subsurface model intercomparison: A first set of benchmark results to diagnose integrated hydrology and feedbacks. Water Resour Res 2014;50(2):1531–49.
[27] Ebel BA, Mirus BB, Heppner CS, Vanderkwaak JE, Loague K. First-order exchange coefficient coupling for simulating surface water–groundwater interactions: parameter sensitivity and consistency with a physics-based approach. Hydrol Proces 2009;23(13):1949–59.
[28] Liggett JE, Werner AD, Simmons CT. Influence of the first-order exchange coefficient on simulation of coupled surface–subsurface flow. J Hydrol 2012;414–415(C):503–15.
[29] Genuchten MV. A closed-form equation for predicting the hydraulic conductivity of unsaturated soils. Soil Sci Soc Am J 1980;44(5):892–8.
[30] Mualem Y. A new model for predicting the hydraulic conductivity of unsaturated porous media. Water Resour Res 1976;12(3):513–22.
[31] Gottardi G, Venutelli M. An accurate time integration method for simplified overland flow models. Adv Water Resour 2008;31(1):173–80.
[32] Hanert E, Legat V. How to save a bad element with weak boundary conditions. Comput Fluids 2006;35(5):477–84.
[33] Bazilevs Y, Hughes T. Weak imposition of Dirichlet boundary conditions in fluid mechanics. Comput Fluids 2007;36(1):12–26.
[34] Simunek J, Sejna M, Genuchten MV. The HYDRUS software package for simulating the two- and three-dimensional movement of water, heat, and multiple solutes in variably-saturated media. Technical manual, PC Progress, Prague, Czech Republic; 2006. p. 1–241.
[35] Saad Y, Schultz MH. GMRES: A generalized minimal residual algorithm for solving nonsymmetric linear systems. SIAM J Sci Stat Comput 1986;7(3):856–-869.
[36] Tian D, Liu D. A new integrated surface and subsurface flows model and its verification. Appl Math Modell 2011;35(7):3574–86.
[37] Abdul A, Gillham R. Laboratory studies of the effects of the capillary fringe on streamflow generation. Water Resour Res 1984;20(6):691–8.
[38] Cloke H, Anderson M, McDonnell J, Renaud J. Using numerical modelling to evaluate the capillary fringe groundwater ridging hypothesis of streamflow generation. J Hydrol 2006;316(1):141–62.
[39] Abdul AS. Experimental and numerical studies of the effect of the capillary fringe on streamflow generation. Ph.D. Thesis, Waterloo (Ontario): University of Waterloo; 1985. p. 210.
[40] Mehl S, Hill M. Grid-size dependence of cauchy boundary conditions used to simulate stream–aquifer interactions. Adv Water Resour 2010;33(4):430–42.
[41] Downer C, Ogden F. Appropriate vertical discretization of richards' equation for twodimensional watershedscale modelling. Hydrol Proces 2004;18(1):1–22.